

# Supramolecular spin valves

M. Urdampilleta<sup>1</sup>, S. Klyatskaya<sup>2</sup>, J-P. Cleuziou<sup>1</sup>, M. Ruben<sup>2,3\*</sup> and W. Wernsdorfer<sup>1\*</sup>

**Magnetic molecules are potential building blocks for the design of spintronic devices<sup>1,2</sup>. Moreover, molecular materials enable the combination of bottom-up processing techniques, for example with conventional top-down nanofabrication<sup>3</sup>. The development of solid-state spintronic devices based on the giant magnetoresistance<sup>4</sup>, tunnel magnetoresistance<sup>5</sup> and spin-valve effects<sup>6</sup> has revolutionized magnetic memory applications. Recently, a significant improvement of the spin-relaxation time has been observed in organic semiconductor tunnel junctions<sup>7,8</sup>, single non-magnetic molecules coupled to magnetic electrodes have shown giant magnetoresistance<sup>9,10</sup> and hybrid devices exploiting the quantum tunnelling properties of single-molecule magnets have been proposed<sup>2</sup>. Herein, we present an original spin-valve device in which a non-magnetic molecular quantum dot, made of a single-walled carbon nanotube contacted with non-magnetic electrodes, is laterally coupled through supramolecular interactions to TbPc<sub>2</sub> single-molecule magnets (Pc = phthalocyanine). Their localized magnetic moments lead to a magnetic field dependence of the electrical transport through the single-walled carbon nanotube, resulting in magnetoresistance ratios up to 300% at temperatures less than 1 K. We thus demonstrate the functionality of a supramolecular spin valve without magnetic leads. Our results open up prospects of new spintronic devices with quantum properties.**

A standard giant magnetoresistance spin valve is an electronic device in which two conducting magnetic layers are separated by a non-magnetic layer. A considerable modification of the electrical conductance through the device can be achieved by altering the electrodes' magnetic configuration (parallel or antiparallel). Because the layers have different magnetic coercivities, in an increasing external magnetic field the magnetization of one layer switches at different field values from the other, that is going from parallel to antiparallel, and finally back to parallel alignment<sup>4</sup>, thus switching the conductance of the device. The resulting magnetoresistance ratio is defined by  $MR = (G_P - G_{AP})/G_{AP}$ , where  $G_P$  and  $G_{AP}$  are the conductances of the spin valve for parallel (P) and antiparallel (AP) alignments. Typical values of MR for metallic spin valves lie in the 10% range at room temperature. A tunnel barrier between the two layers leads to MR values greater than 100%, for instance, in commercially used spin valves in read heads. The two magnetic layers can be also connected through a carbon nanotube, leading to typical MR values of about 3% for PdNi or permalloy single-walled carbon nanotube (SWCNT) spin valves<sup>11,12</sup> and 60% for La<sub>(1-x)</sub>Sr<sub>x</sub>MnO<sub>3</sub> (LSMO)-based electrodes<sup>13</sup>. In all these devices, the active layers are classical magnets.

An alternative experimental set-up proposes to use quantum nanomagnets<sup>2</sup>. It was suggested that if a single-molecule magnet (SMM) is laterally coupled to an electrically contacted SWCNT,

its highly anisotropic magnetic moment may influence the current passing through the SWCNT, thus permitting the readout of the molecular magnetic state by standard conductance measurements. This idea is experimentally realized here. We have measured high magnetoresistance ratios in this supramolecular SMM-SWCNT geometry, in which single quantum nanomagnets act as both magnetic polarizers and analysers. Remarkably, the presented experimental results demonstrate the electrical detection of the magnetization switching of a single quantum magnet. Out of 130 investigated devices, 25 samples showed signals due to magnetic molecules. Seven devices were studied in detail and exemplary data for one of them are presented below (concerning other samples, see Supplementary Figs S2 and S3).

The rare-earth-based SMMs are among the most promising systems for molecular spintronic applications. In *bis*-phthalocyaninato-terbium (III) complexes, hereafter TbPc<sub>2</sub> (ref. 14), the total magnetic moment is given by  $J = 6$  and originates from both orbital and spin contributions<sup>15</sup>. In its neutral form the TbPc<sub>2</sub> molecule represents a two-spin system: the Tb<sup>3+</sup> ion has an intrinsic magnetic anisotropy whereas the organic spin  $S = 1/2$  radical is delocalized over the two phthalocyanine ligands enhancing the magnetic coupling to the environment (Fig. 1a). At low temperatures, quantum magnets of the TbPc<sub>2</sub> family are characterized by (1) a large magnetic moment in the ground state, (2) a high zero-field splitting due to their large magnetic anisotropy, (3) slow relaxation of the magnetization and (4) a strong hyperfine coupling<sup>16</sup>. In addition, their magnetic properties show a very large spectrum of quantum physics phenomena<sup>17</sup>, for example quantum tunnelling of magnetization (QTM) between up and down magnetization polarizations and quantum interference between different tunnelling paths<sup>18</sup>.

The investigation of the magnetic characteristics of the TbPc<sub>2</sub> SMM crystal, using a micro superconducting quantum interference device at 0.04 K (ref. 19), reveals a hysteresis loop containing magnetic quantum phenomena (Fig. 1b; ref. 16). The sharp steps within the magnetic hysteresis loop originate from quantum tunnelling at the respective energy-level crossings (Fig. 1c). Due to the large magnetic anisotropy of the Tb<sup>3+</sup> ion, the ground-state doublet with quantum numbers  $J_z = \pm 6$  is well separated from the excited states by several hundred Kelvin (see Supplementary Fig. S1; refs 20,21). Moreover, the interaction of each ground state with the four nuclear-spin states of the Tb<sup>3+</sup> ion nuclear spin ( $I = 3/2$ ) leads to several energy-level crossings and therefore QTM. A further magnetization-reversal mechanism, occurring at higher field, is given by the direct relaxation process, which can be seen as a non-coherent tunnelling event combined with a phonon emission. Therefore, a TbPc<sub>2</sub> SMM can switch at different external fields, depending on the mechanism involved in the magnetization reversal (see Supplementary Fig. S4a and b). Recently, it has

<sup>1</sup>Institut Néel, CNRS et Université Joseph Fourier, BP 166, F-38042 Grenoble Cedex 9, France, <sup>2</sup>Institute of Nanotechnology (INT), Karlsruhe Institute of Technology (KIT), 76344 Eggenstein-Leopoldshafen, Germany, <sup>3</sup>Institute de Physique et Chimie de Matériaux de Strasbourg (IPCMS), CNRS-Université de Strasbourg, 67034 Strasbourg, France. \*e-mail: mario.ruben@kit.edu; wolfgang.wernsdorfer@grenoble.cnrs.fr.

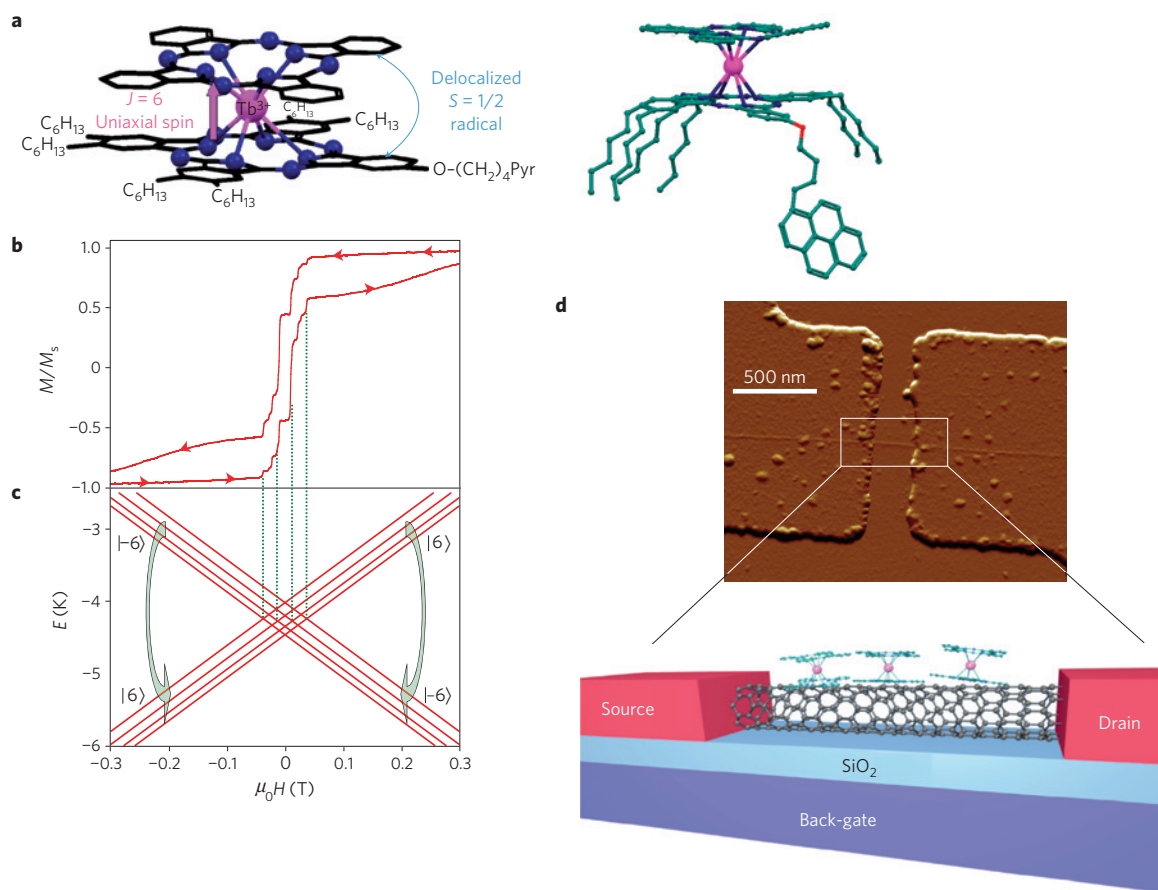


**Figure 1 | Supramolecular spin-valve device.** **a**, Schematic and molecular representation of the TbPc<sub>2</sub>\* quantum nanomagnet. A Tb<sup>3+</sup> ion (pink) is coordinated by two phthalocyanine groups; pyrenyl and hexyl substitutions maximize the supramolecular interaction with sp<sup>2</sup>-carbon materials. The quantum magnet consists of two spin systems: an organic S = 1/2 radical delocalized over the two phthalocyanine rings and a highly anisotropic J = 6 spin system localized on the Tb<sup>3+</sup> metal ion. **b**, Magnetic characteristics of the TbPc<sub>2</sub>\* SMM showing the hysteresis loop at 0.04 K for a single crystal of diluted sample measured with a micro superconducting quantum interference device set-up at a field sweep rate of 1 mT s<sup>-1</sup>. The marked steps are induced by quantum tunnelling at energy-level crossings presented in **c**. **c**, Zeeman diagram for the lowest states with J<sub>z</sub> = ±6, which are split by the four nuclear spin states of I = 3/2. The calculation was done with the ligand field parameters of ref. 16. **d**, Top, atomic force micrograph of the supramolecular spin valve. The single-walled nanotube lies on a SiO<sub>2</sub> surface supported by a back gate and is connected to palladium source and drain electrodes. **d**, Bottom, scheme of the supramolecular spin-valve architecture (hexyl and pyrenyl groups are omitted for reasons of clarity).

been shown that the prominent magnetic properties of TbPc<sub>2</sub> SMMs remain robust when attached through supramolecular π–π interactions to sp<sup>2</sup>-carbon materials, such as carbon nanotubes<sup>22</sup> and graphene<sup>23</sup>. However, it is important to note that each molecule when deposited on the nanotube relaxes into a slightly different supramolecular position, leading to a local variation of the physical properties. As a matter of fact, some of them would have a huge QTM probability whereas others would mostly undergo a direct relaxation process.

To increase the non-invasive attachment to SWNTs at very low concentrations, the TbPc<sub>2</sub> SMMs used herein were modified by introducing one pyrene group and six hexyl groups into one of the two Pc rings (referred to hereafter as TbPc<sub>2</sub>\*; see Fig. 1a). Both the pyrene group and the alkyl chains are known to exhibit attractive van der Waals interactions with sp<sup>2</sup>-carbon materials and are used as anchoring points on the nanotube. Moreover, the steric hindrance induced by this ligand prevents recrystallization of the SMM on the nanotube. The anchoring groups steer the supramolecular grafting of the quantum magnet and bring the substituted Pc ring into direct contact with the SWCNT wall. The latter and the Pc ring are conjugated systems, which strongly hybridize through π–π interactions<sup>24</sup>. The supramolecular sample geometry is shown in Fig. 1d. The external magnetic field is

applied in the plane of the sample (0° corresponds to the normal to the nanotube axis) and a back gate fine-tunes the chemical potential of the SWCNT. Figure 2 shows the electronic-transport characteristics of the supramolecular TbPc<sub>2</sub>\*–SWCNT set-up. Differential conductance maps of dI/dV as a function of source–drain voltage V<sub>sd</sub> and back-gate voltage V<sub>g</sub> were taken at 0 T (Fig. 2a) and 1 T (Fig. 2b), corresponding to random and polarized orientations of the TbPc<sub>2</sub>\* magnetic moments, respectively. At both magnetic fields, the differential conductance maps exhibit the features of Coulomb diamonds<sup>25</sup>, typically observed for SWCNT quantum dots in the weak-coupling regime<sup>26</sup>. Intriguingly, the degeneracy points of most of the Coulomb diamonds are open in the absence of an external magnetic field (0 T, Fig. 2a) and closed in its presence (1 T, Fig. 2b). This is clear evidence of the modulation of an extra tunnelling barrier inside the quantum dot. Further insight can be gained when measuring the magnetic field hysteresis loops of the conductance at V<sub>sd</sub> = 0. In Fig. 2c, the magnetic field is swept between 1 and –1 T resulting in an abrupt switch between a relatively high value (~1 μS) and a lower one (~100 nS). The characteristics of the hysteresis loops are consistent for each of the Coulomb peaks, as shown in Fig. 2d: the difference in conductance value is plotted between trace (from –1 to 1 T) and retrace (from 1 to –1 T) for each

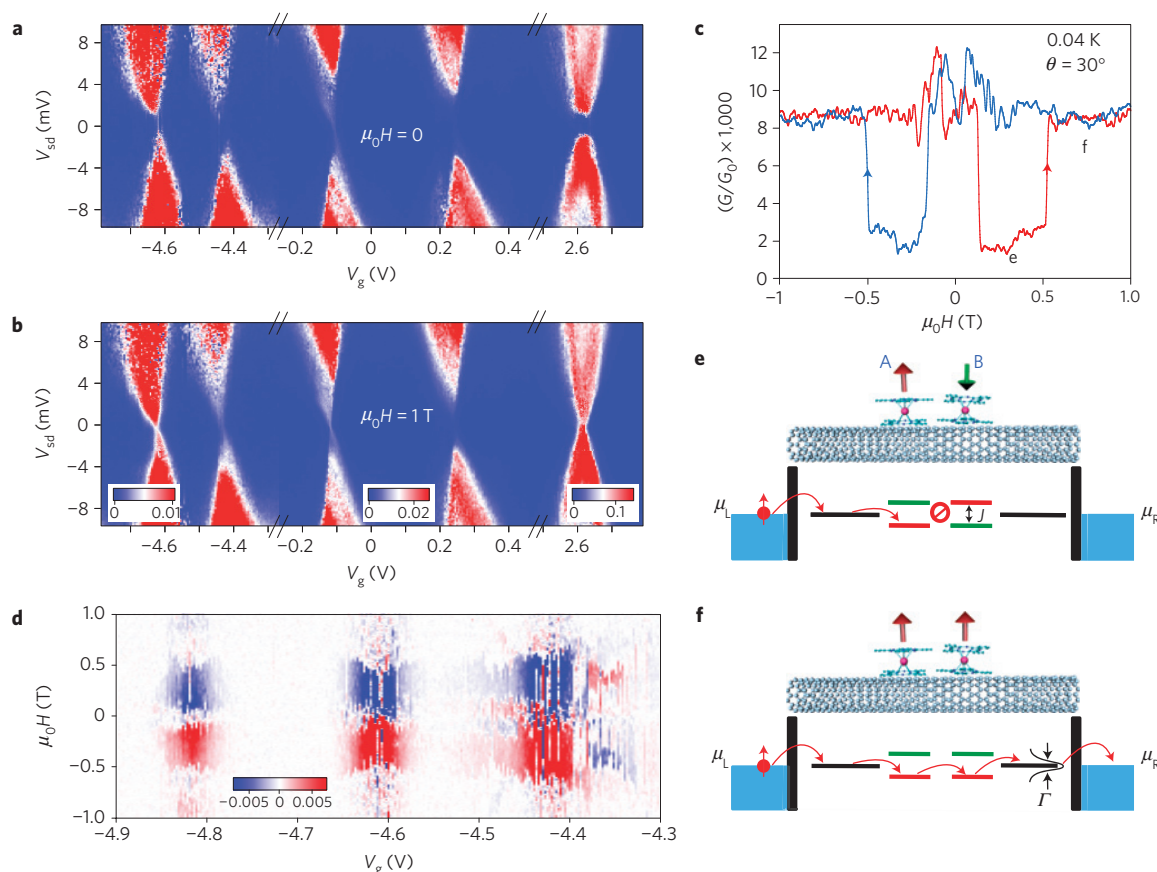


**Figure 2 | Molecular spin-valve electronic-transport characteristics.** **a**, Coulomb map of the differential conductance as a function of source-drain voltage  $V_{sd}$  and back-gate voltage  $V_g$  without magnetic field. The differential conductance is given in the unit of the conductance quantum  $G_0$ . A gap  $\Delta$  is induced at the degeneracy point when all the magnetic moments are randomly oriented. Magnetic molecules induce effective tunnelling barriers in the SWCNT, hindering the electron flow, except in the case where the electrons have enough energy ( $V_{sd} > \Delta/2$ ) to overcome these barriers. **b**, Coulomb map under a magnetic field of 1 T. The gap is closed, and the standard degeneracy points are recovered. This corresponds to the situation where all molecules are polarized in approximately the same direction. **c**, Zero-bias conductance measured as a function of the magnetic field. The red curve corresponds to the conductance under increasing field ( $-1$  to  $+1$  T) and the blue curve under decreasing field. The conductance jumps around zero field are attributed to molecules experiencing quantum tunnelling due to tunnel splittings. The last jumps around  $\pm 500$  mT are attributed to a direct relaxation process of a single molecule. When all the magnetic momenta are parallel only one spin carrier can flow easily, whereas when the magnetic moment are antiparallel the electron flow of both spin carriers is hindered. **d**, Intensity of the conductance hysteresis measured as a function of the gate voltage. The colour code corresponds to the difference between magnetic field trace and retrace, given in the unit of  $G_0$ : blue corresponds to negative values, red to positive and white to zero hysteresis. The most intense regions are directly correlated to the Coulomb peaks. **e, f**, Schematic representation of the mechanism involving two  $\text{TbPc}_2^*$  SMM molecules (A and B) grafted on an SWCNT. With increasing magnetic field, molecule A switches first (**e**), thus leading to an antiparallel configuration of the spin valve with lowest conductance. Each molecule induces localized states in the nanotube through exchange interaction. The value of this interaction is estimated to be around  $J = 0.5$  meV. The mismatch between spin levels induces effective tunnel barriers in the SWCNT for both spin polarizations. As a result, the electron flow through the SWCNT is hindered. When molecule B switches (**f**), a parallel configuration is recovered, and because of the level broadening ( $\sim 0.2$  meV) this configuration leads to high conductance. The hexyl and pyrenyl groups of the  $\text{TbPc}_2^*$  SMM are omitted for reasons of clarity.

gate step. The hysteretic behaviour disappears above a bias voltage of about 0.5 mV.

To relate the device characteristics to the magnetic signature of the  $\text{TbPc}_2^*$  quantum magnets, a detailed investigation of the magnetic field dependence of the largest conductance jumps was carried out. An analysis of the angular dependence of the switching field, which was made by plotting the difference between the trace and the retrace, reveals a very pronounced dependence. The smallest switching fields, which define the easy axis of magnetization, were found to be orthogonal to the SWCNT axis ( $x$  direction), whereas along the tube axis ( $y$  direction) a hard axis was found (Fig. 3a). Such a very strong angular dependence is in agreement with the Ising-like uniaxial anisotropy of the  $\text{TbPc}_2$ -SMM family<sup>16</sup>. We compared the orientation of the easy axis with the SWCNT axis and found that the  $\text{TbPc}_2^*$  molecule is orientated with the Pc rings

parallel to the SWCNT wall, which is in accordance with the supramolecular design maximizing the  $\pi$ - $\pi$  interactions between the Pc ring and the nanotube.

Quantum tunnelling of magnetization is an inherently stochastic process: the magnetization reversal at a tunnel splitting or through a direct relaxation process is expressed by transition probabilities. By cycling the hysteresis loop many times, the related stochastics of the magnetic moment reversal can be elucidated (Fig. 3b). Increasing temperatures lead to a continuous reduction of the area of the hysteresis loop (Fig. 3c). At 40 mK the switching field is found to be around 0.5 T progressively declining and finally vanishing above 600 mK. The blocking temperature can be extrapolated to be around 1 K, which is in good agreement with recent reports on a  $\text{TbPc}_2$  submonolayer<sup>27</sup>. Other samples showed similar temperature dependencies (see Supplementary Fig. S5).

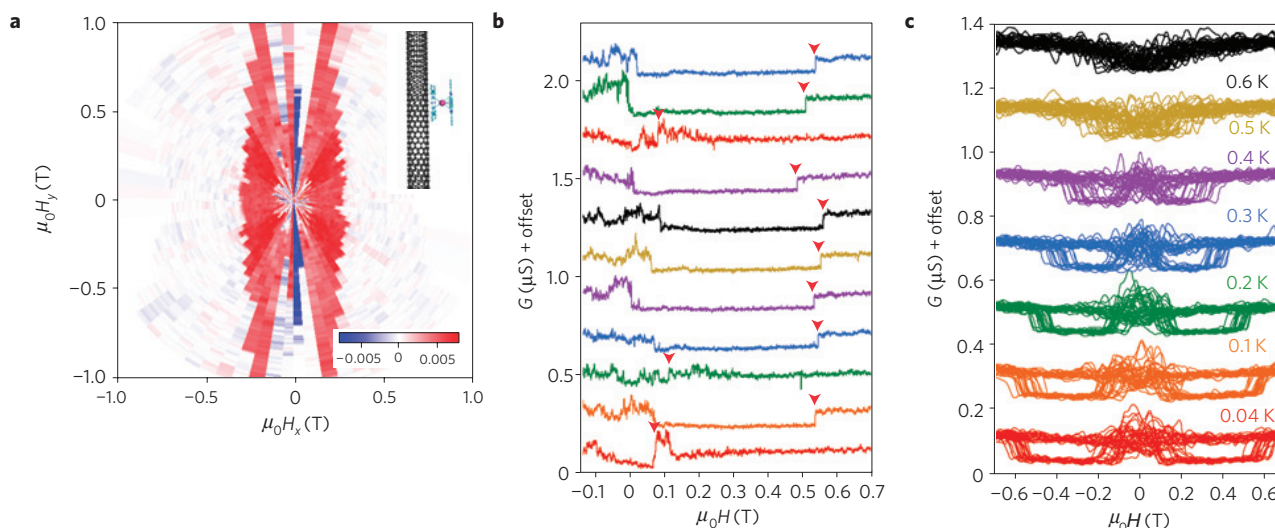


**Figure 3 | Molecular spin-valve switching-field characteristics.** **a**, Angular dependence of the switching field corresponding to the direct relaxation process. The difference between trace (from  $-1$  to  $+1$  T) and retrace (from  $+1$  to  $-1$  T) is plotted as a function of the angle of the applied field. The colour code is given in  $G_0$ . The white code corresponds to no difference between trace and retrace for the corresponding field value whereas a red code corresponds to a bistable region. This means that in the white region both molecules are polarized in the same way and in the red region the antiparallel configuration is adopted. As a result, the border between the white and the red region corresponds to the switching field of the molecule experiencing a direct relaxation process. It is important to note that the switching field along the  $y$  axis cannot be resolved because our magnets are limited to 1 T. This ellipsoidal behaviour has been measured repeatedly on several samples (see Supplementary Fig. S3), and is in agreement with the Ising-like uniaxial anisotropy of the  $\text{TbPc}_2^*$ . The  $x$  axis can be attributed to the easy axis and the  $y$  axis to the hard axis. By comparing the orientation of the easy axis with the nanotube direction it can be deduced that the  $\text{TbPc}_2^*$  molecule is flat-landing on the nanotube, as shown in the inset. **b**, The conductance is measured 11 times as a function of the magnetic field applied at an angle of  $30^\circ$  with a sweep rate of  $2 \text{ mT s}^{-1}$ . The switching field of the studied molecule is marked by an arrow. Some of the curves present a transition close to zero instead of 0.5 T. This is attributed to a tunnel mechanism at an avoided level crossing. In this case all the  $\text{TbPc}_2^*$  molecules have experienced a tunnel transition and the spin-valve behaviour disappears. Most of the tunnel transitions happen at small positive field values, establishing that the Tb nuclear spins are cold enough to involve mainly the lowest magnetic spin states. **c**, 20 hysteresis loops at several temperatures between 0.04 and 0.6 K, using a field sweep rate of  $70 \text{ mT s}^{-1}$ . A few molecules switch around zero field through a tunnel process whereas one molecule switches at higher fields through a direct relaxation process. The blocking temperature is extrapolated to be around 1 K.

The observation of electronic coupling of the terbium-based  $J = 6$  magnetic moment with the conduction electrons is explained by the intermediating presence of the  $S = 1/2$   $\pi$  radical delocalized on the organic phthalocyanine ring systems. Owing to  $\pi$ - $\pi$  interaction, this radical is supposed to be in close electronic contact with surfaces; for example, it was shown to lead to Kondo features in scanning probe spectroscopy studies<sup>28</sup>. This means that the wavefunction of this unpaired spin can easily hybridize with the  $\pi$ -electron density of the nanotube. Moreover, transition-metal/Pc systems adsorbed on  $sp^2$ -graphite surfaces show a pinning of the lowest unoccupied molecular orbital level close to the Fermi level<sup>29</sup> and recent investigations have shown a weak antiferromagnetic exchange coupling of the Tb magnetic moment of  $\text{TbPc}_2$  to a ferromagnetic Ni substrate (P. Gambardella *et al.*, manuscript in preparation). Furthermore, the radical ligand state is close in energy to the Tb  $4f$  states<sup>30</sup>, enabling an efficient coupling of the Tb magnetic  $J = 6$  state with the conduction electron of the SWCNT.

The observed magnetoresistance behaviour is explained by an effective tunnelling barrier induced by the magnetic configuration of very few SMMs coupled to the SWCNT quantum dot. The average number of molecules was previously determined to be about four molecules for a source-drain SWCNT segment of 300 nm (ref. 23). The conduction electrons of the SWCNTs are locally influenced through the  $\pi$ -radical-mediated exchange mechanism (*vide supra*) of the confined  $\text{TbPc}_2^*$  magnetic moment. For reasons of simplicity, the mechanism will be explained for the most ideal case involving two SMM molecules (A and B, Fig. 2e,f) and one spin-degenerate conduction channel: each molecule locally lifts the spin degeneracy, and as a result there is an energy mismatch in the antiparallel configuration between the orbitals

of the same spin, which creates an effective tunnelling barrier. In a spin-valve picture, the first of the molecules (A) plays the role of spin polarizer, whereas the second one (B) acts as spin analyser. The presence of two reversal mechanisms (tunnel splitting versus direct relaxation process) expressing significantly different tunnelling probabilities (see Supplementary Fig. S4a and b) leads to different switching fields for quantum magnets A and B. In the example presented herein molecule A has a close-to-unit QTM probability around zero field (but spread due to the hyperfine coupling) and consequently exhibits magnetic-moment flips close to zero field (Fig. 2e). With increasing magnetic field, the second molecule (B) remains still in the opposite magnetic state, rendering an antiparallel configuration of the spin valve, until this second molecule experiences a direct transition (Fig. 2f), reprogramming the valve into its parallel configuration. Moreover, the quantum behaviour of the second molecule (B) has been investigated through its magnetic field sweep-rate dependence (see Supplementary Fig. S4a). With decreasing fields, around a rate of  $2 \text{ mT s}^{-1}$ , the spin-valve characteristic disappears in one-third of the cases, which is in accordance with the Landau-Zener theory<sup>18</sup>. When molecules A and B tunnel close to zero field, the spin-valve behaviour vanishes (Fig. 3b). The supramolecular spin valve described here thus offers two distinct working regimes: (1) a bi-stable and (2) a sweeping-rate-independent regime. This allows for functional fine-tuning as well as electronic detection and manipulation of a single magnetic moment. It should be noted that other mechanisms invoking any shift of the Coulomb diamond to explain conductance changes (for example magneto-Coulomb effect, see Supplementary Fig. S6) are refuted by Fig. 2d, where no change of the magnetoconductance sign is observed.

In conclusion, a supramolecular spin valve consisting of quantum magnets (SMMs) and SWCNT components has been demonstrated. On reversing the magnetic field, the device exhibits magnetoresistance ratios up to 300%. Analysis of the differential conductance of the SWCNT with the switching-field angle and temperature reveals fingerprint-like characteristics of the magnetic molecules exhibiting Ising-like uniaxial anisotropy and quantum tunnelling phenomena. Our results open a pathway towards the design of operable molecular spintronic devices projecting the implementation of new electrical functionalities, high integration depth and an alternative fabrication scheme to cost-intensive lithographic technologies.

## Methods

**Sample preparation.** SWCNTs of diameter about  $\sim 1.2$  nm grown by the laser ablation method at the Rice University were dispersed in 1–2 ml dichloroethane and sonicated for 1 h. A droplet of this suspension was deposited onto a degenerately doped p-type silicon wafer with a  $\sim 450$  nm surface oxide. SWCNTs were located by atomic force microscopy with respect to predefined markers and then contacted with 50-nm-thick Pd by standard electron-beam lithography with a contact spacing of  $\sim 300$  nm. The  $\text{TbPc}_2^*$  SMMs were synthesized as previously reported<sup>22</sup>. The supramolecular grafting was carried out by drop casting a solution of  $\text{TbPc}_2^*$  diluted in dichloromethane with molarity  $M = 10^{-8}$  mol l<sup>-1</sup> onto the sample. After 5 s, the sample was rinsed in dichloromethane and dried under nitrogen flow. Residual dichloromethane was removed by a second rinse with isopropanol.

**Conductance experiments.** Samples with high resistance ( $>100$  k $\Omega$ ) at room temperature were selected. The conductance measurements were carried out in a  $^3\text{He}/^4\text{He}$  dilution refrigerator with a base temperature of 30 mK. Identical stable spin-valve characteristics have been seen on two different samples using this method and on five samples with the same method but with nanotubes grown by chemical vapour deposition (see Supplementary Section S2). The magnetic field in the sample plane was provided by two magnets, generating up to 1 T and up to 0.7 T, respectively. Electrical measurements of interest were made using a Stanford Research Systems SR-830-DSP lock-in amplifier or an ADwin real-time data acquisition system.

Received 16 February 2011; accepted 17 May 2011; published online 19 June 2011

## References

- Rocha, A. R. *et al.* Towards molecular spintronics. *Nature Mater.* **4**, 335–339 (2005).
- Bogani, L. & Wernsdorfer, W. Molecular spintronics using single-molecule magnets. *Nature Mater.* **7**, 179–186 (2008).
- Lehn, J.-M. Supramolecular chemistry: From molecular information toward self-organization and complex matter. *Rep. Prog. Phys.* **67**, 249–265 (2004).
- Baibich, M. N. *et al.* Giant magnetoresistance of (001)Fe/(001)Cr magnetic superlattices. *Phys. Rev. Lett.* **61**, 2472–2475 (1988).
- Binasch, G., Grünberg, P., Saurenbach, F. & Zinn, W. Enhanced magnetoresistance in Fe–Cr layered structures with antiferromagnetic interlayer exchange. *Phys. Rev. B* **39**, 4828–4830 (1989).
- Dieny, B. Giant magnetoresistive in soft ferromagnetic multilayers. *Phys. Rev. B* **43**, 1297–1300 (1991).
- Awschalom, D. D. & Flatté, M. M. Challenges for semiconductor spintronics. *Nature Phys.* **3**, 153–159 (2007).
- Dediu, V., Hueso, L., Bergenti, I. & Taliani, C. Spin routes in organic semiconductors. *Nature Mater.* **8**, 707–716 (2009).
- Brede, J. *et al.* Spin- and energy-dependent tunnelling through a single molecule with intramolecular spatial resolution. *Phys. Rev. Lett.* **105**, 047204 (2010).
- Schmaus, S. *et al.* Giant magnetoresistance through a single molecule. *Nature Nanotech.* **6**, 185–189 (2011).
- Sahoo, S. *et al.* Electric field control of spin transport. *Nature Phys.* **1**, 99–102 (2005).
- Aurich, H. *et al.* Permalloy-based carbon nanotube spin-valve. *Appl. Phys. Lett.* **97**, 153116 (2010).
- Hueso, L. *et al.* Transformation of spin information into large electrical signals using carbon nanotubes. *Nature* **445**, 410–413 (2007).

- Ishikawa, N. *et al.* Upward temperature shift of the intrinsic phase lag of the magnetization of bis(phthalocyaninato)terbium by ligand oxidation creating an  $S = 1/2$  spin. *Inorg. Chem.* **43**, 5498–5500 (2004).
- Stepanow, S. *et al.* Spin and orbital magnetic moment anisotropies of monodispersed bis(phthalocyaninato) terbium on a copper surface. *J. Am. Chem. Soc.* **132**, 11900–11901 (2010).
- Ishikawa, N., Sugita, M. & Wernsdorfer, W. Quantum tunnelling of magnetization in lanthanide single-molecule magnets: bis(phthalocyaninato)terbium and bis(phthalocyaninato)dysprosium anions. *Angew. Chem. Int. Edn.* **44**, 2931–2935 (2005).
- Christou, G., Gatteschi, D., Hendrickson, D. N. & Sessoli, R. Single-molecule magnets. *MRS Bull.* **25**, 66–71 (2000).
- Wernsdorfer, W. & Sessoli, R. Quantum phase interference and parity effects in magnetic molecular clusters. *Science* **284**, 133–135 (1999).
- Wernsdorfer, W. From micro- to nano-SQUIDS: Applications to nanomagnetism. *Supercond. Sci. Technol.* **22**, 064013 (2009).
- Ishikawa, N. *et al.* Determination of ligand-Field parameters and f electronic structures of double-decker bis(phthalocyaninato)lanthanide complexes. *Inorg. Chem.* **42**, 2440–2446 (2003).
- Zopellaro, G. *et al.* Spin dynamics in the negatively charged terbium (III) bis phthalocyaninato complex. *J. Am. Chem. Soc.* **131**, 4387–4396 (2009).
- Klyatskaya, S. *et al.* Anchoring of rare-earth-based single-molecule magnets on single-walled carbon nanotubes. *J. Am. Chem. Soc.* **131**, 15143–15151 (2009).
- Lopes, M. *et al.* Surface-enhanced Raman signal for terbium single-molecule magnets grafted on graphene. *ACS Nano* **4**, 7531–7537 (2010).
- Wang, Y. Y. *et al.* Single-walled carbon nanotube/cobalt phthalocyanine derivative hybrid material: Preparation, characterization and its gas sensing properties. *J. Mater. Chem.* **21**, 3779–3787 (2011).
- Hanson, R., Kouwenhoven, L. P., Petta, J. R., Tarucha, S. & Vandersypen, L. M. K. Spins in few-electron quantum dots. *Rev. Mod. Phys.* **79**, 1217–1265 (2007).
- Sapmaz, S., Jarillo-Herrero, P., Kouwenhoven, L. P. & van der Zant, H. S. J. Quantum dots in carbon nanotubes. *Semicond. Sci. Technol.* **21**, S52–S63 (2006).
- Otero, L. M., Caneschi, A. & Sessoli, R. X-Ray detected magnetic hysteresis of thermally evaporated terbium double-decker oriented films. *Adv. Mater.* **42**, 5488–5493 (2010).
- Katoh, K. *et al.* Direct observation of lanthanide(III)-phthalocyanine molecules on Au(111) by using scanning tunnelling microscopy and scanning tunnelling spectroscopy and thin-film field-effect transistor properties of Tb(III)- and Dy(III)-phthalocyanine molecules. *J. Am. Chem. Soc.* **131**, 9967–9971 (2009).
- Gopakumar, T. G., Müller, F. & Hietschold, M. STM and STS studies of planar and non-planar naphthalocyanines on graphite I & II. *J. Phys. Chem. B* **110**, 6051–6060 (2006).
- Vitali, L. *et al.* Electronic structure of surface-supported bis(phthalocyaninato) terbium(III) single molecular magnets. *Nano Lett.* **8**, 3364–3368 (2008).

## Acknowledgements

This work is partially supported by the DFG programmes SPP 1459 and TRR 88, ANR-PNANO project MolNanoSpin No ANR-08-NANO-002, ERC Advanced Grant MolNanoSpin No 226558, STEP MolSpinQIP and the Nanosciences Foundation of Grenoble. Samples were fabricated in the NANOFAB facility of the Néel Institute. We thank M. Affronte, F. Balestro, N. Bendiab, L. Bogani, E. Bonet, V. Bouchiat, L. Calvet, A. Candini, D. Feinberg, J. Jarvinen, L. Marty, T. Novotny, R. Piquetel, C. Thirion and R. Vincent for discussion and software development. We thank D. Lepoittevin, E. Eyraud, R. Haettel, C. Hoarau and V. Reita for technical support. We thank N.-V. Nguyen and T. Crozes for help in device fabrication.

## Author contributions

M.U., M.R. and W.W. designed, carried out and analysed the experiments; J.-P.C. helped to fabricate the devices; S.K. and M.R. designed, synthesized and characterized the molecule; M.U., M.R. and W.W. co-wrote the paper.

## Additional information

The authors declare no competing financial interests. Supplementary information accompanies this paper on [www.nature.com/naturematerials](http://www.nature.com/naturematerials). Reprints and permissions information is available online at <http://www.nature.com/reprints>. Correspondence and requests for materials should be addressed to M.R. or W.W.